

Power Handling of Slot Loop Frequency Selective Surface Based on Approximate Analytical Method

Kang Luo, Jin Meng*, Danni Zhu, and Jiangfeng Han

National Key Laboratory of Electromagnetic Energy, Naval University of Engineering, Wuhan 430000, China

ABSTRACT: In this paper, the power handling of a slot loop frequency selective surface based on approximate analytical method is proposed. The physical nature of the slot array periodic moment method is derived in detail. It is found that the left and right sides of periodic scatter matrix respectively represent the total tangential magnetic field acting on the left and the right magnetic dipole arrays and moving in the direction of the reference array. According to the principle of equivalence, a slot array can be modeled by an array of magnetic currents on each side of the perfect electronic conductor. As a result, the total tangential magnetic field is zero in the sense of physical concept. Furthermore, a simple sinusoidal function is then used to approximate the magnetic current distribution along the slot loop which is similar to that of dipole antenna. By studying the corresponding zero points and extreme point of the magnetic current for the slot loop frequency selective surface element, the transmission coefficients and maximum electronic field are calculated. Examples of rectangle and triangle slot ring frequency selective surface have verified the efficiency and accuracy of the proposed method.

1. INTRODUCTION

Frequency selective surface plays a core role in the field of modern radio systems. The reflecting and transmitting of waves in a periodic structure is a typical issue. Periodic elements composed of a square loop and slot have been widely applied in frequency selective surface (FSS), such as radomes, absorbers, and dual band antennas sub-reflectors. The filter characteristic is usually simulated by full-wave codes (e.g., finite element method (FEM), finite-difference time-domain (FDTD), method of moments (MoM)) and the corresponding commercial electromagnetic software (e.g., HFSS, CST, Comsol, FEKO). In the same time, a variety of equivalent circuit or network methods for the efficient analysis of FSS have been studied, as well as the approximate analytical methods [1, 2].

The initial attempt to predict the transmission loss for FSS of square loop under normal incidence is proposed by Langley and Parker [3]. According to waveguide discontinuities proposed by Marcuvitz [4], the impedance of periodic elements of relatively narrow continuous strips can be equivalent as inductive and capacitive components. The equivalent network topology consists of series and parallel resonant circuit which can then be established based on the geometric of the element. The transmission characteristics under oblique incidence angles and cross-polarization are also discussed. The model is then extended to the double square [5] strips FSS and triple square strips broadband radar absorber [6]. A further equivalent circuit model optimization with consideration of the physical attributes for periodic square slot and strip is presented in [7, 8]. However, this kind of models is limited to relatively thick substrate and small incidence angle. Besides, the equivalent network needs to be adjusted and optimized for complex periodic structures. Although a simple and efficient equivalent circuit

model based on first-order circuit approach for FSS can be established following [9], the corresponding circuit parameters have to be computed by full-wave electromagnetic field numerical calculation method.

A fully analytical and accurate multimodal equivalent network method is presented in [10, 11]. This modal is also inspired by the equations given by Marcuvitz, while the harmonics of the Floquet analysis is recognized as the modes of the generalized waveguide, and a microwave network approach can then be used. Both the approaches for 1-D and 2-D periodic structures have been studied. It has also been extended to the analysis of sub-wavelength holes and negative index medium. Another classical fully analytical method based on the mutual impedance approach (the element to element approach) and the plane wave expansion (the spectral approach) is proposed by Munk [12], namely the periodic moment method (PMM). This scheme has discussed all the practical problems and application for FSS, such as the hybrid radome, band-stop filter, circuit analog absorbers, and power handling of periodic surfaces. These two analytical methods need to obtain the current distribution in advance (the same as other methods). The equivalent network method only considers some simple rectangular scatters. The approximate closed form expressions for aperture field and patch surface current profiles have been obtained. For complex element, a full-wave simulation is necessary. PMM method solves the problem by the mutual impedance approach which is closely associated with the method of moments. However, it results in a high-order matrix equation which is time consuming to solve [13, 14]. Although the current distribution of the FSS element can be calculated by full-wave simulation, the equivalent circuit method (e.g., theory of Maxwellian circuits proposed by Mei [15–17] and antenna current proposed by Schelkunoff and Friis [18]) is also efficient. Besides, it pro-

* Corresponding author: Jin Meng (mengjingemc@163.com).

TABLE 1. Typical analysis methods for FSS.

Ref.	Method	Efficiency	Field calculation	Scope of application
[1]	analytical/multimodal equivalent network	high	unavailable	arbitrary structure
[2]	numerical/FDTD	moderate	available	arbitrary structure
[3]	analytical/quasi-static equivalent circuit	high	unavailable	relatively simple structure
[13]	analytical/PMM and Kirchhoff circuit	high	available	planar structure with narrow strip/slots
[19]	numerical/HFSS	low	available	arbitrary structure

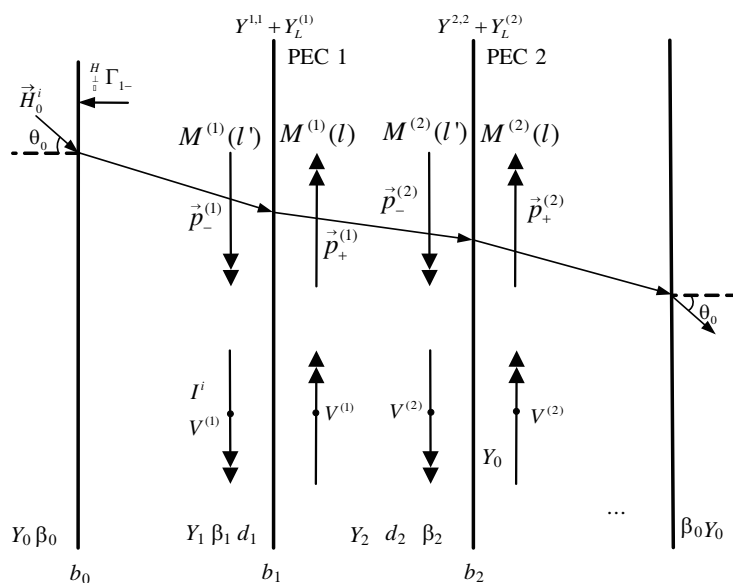


FIGURE 1. Equivalent model of multi-layer slot array.

vides physical nature of the current distribution which is similar to the analysis of transmission line. However, there are few research on FSS power handling [19–22]. Table 1 provides a summary of typical FSS analysis methods.

In this paper, an efficient equivalent transmission line method based on Munk’s scheme for loop-type FSS power handling is proposed. In what follows, first the breakdown principle of a slot type FSS corresponding to PMM equation is deduced (Section 2). Then, according to the full wave simulation and analysis of the equivalent transmission line, the sinusoidal function is proposed to approximate the current distribution on the strip ring FSS which can further obtain the magnetic current on the slot ring FSS by duality principle (Section 3). Besides, the associated magnetic current distribution is further applied to calculate the maximum electronic of the slot element. Two examples have verified the efficiency and accuracy of the proposed method.

2. BREAKDOWN PRINCIPLE OF SLOT ARRAY

The incident electric field \vec{E}^i is analyzed in terms of patch array, with the incident magnetic field \vec{H}^i in terms of slot array. As shown in Fig. 1, the left side of the array generates a total reflection field, and the right side generates a total transmission field. There is a total field distribution in the dielectric

layer. These fields are consistent with those calculated by periodic FDTD. The introduction of the incident wave from the connecting boundary of total/scattered field in the free space on the left side of the array helps calculate the total tangential electric field on the slot of each array and makes the field equivalent to a magnetic current so as to establish an equivalent model of the slot array.

The equivalent model is equivalently handled gradually from left to right. According to the principle of equivalence, a slot array can be modeled by an array of magnetic currents on each side of the PEC. The equivalent magnetic currents are the total tangential electric field at the original slot. The equivalent model of the multi-layer slot array is shown in Fig. 1.

In Fig. 1, both $\vec{P}^{(1)}$ and $\vec{P}^{(2)}$ represent the direction of the corresponding reference element and both $M^{(1)}(l)$ and $M^{(2)}(l)$ the distribution of corresponding receiving currents. Initially, the wave is transmitted from left to right through the slot in the array, including multiple reflection of the medium. Based on the equivalent network, the elements on the left side of array 1 generates induced current I^i under the action of the incident wave \vec{H}_0^i . I^i is the excitation source of each element on the right side of array 1. The mutual admittance only exists between the adjacent arrays. In consequence, the transmitted field only comes from the last slot array. The equation for the equivalent network in Fig. 1 cannot be directly derived from

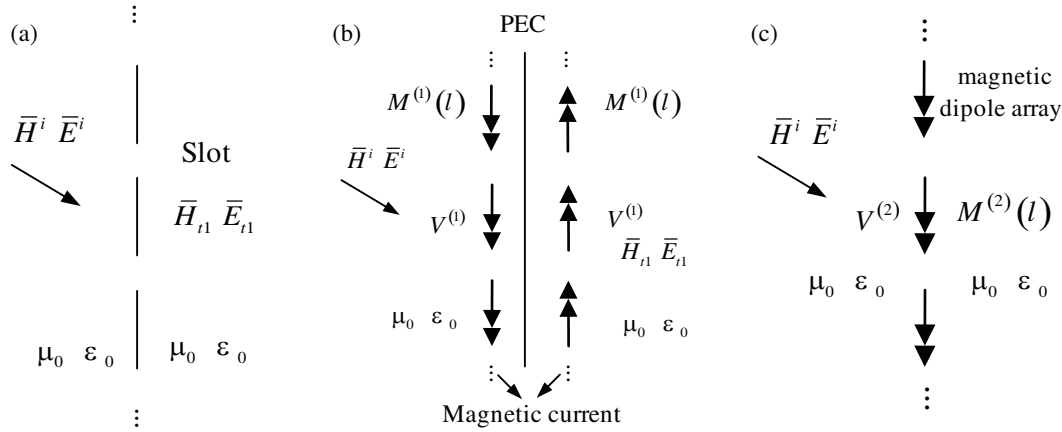


FIGURE 2. Equivalent model of a single slot array in free space. (a) Original slot array. (b) Complementary surface. (c) Babinet's principle.

strip array for the network. That is because there is difference in structure between the two and also the concept of admittance and solution.

Babinet's principle and the duality principle are used to derive the network equations of the slot array [7]. Therefore, the equivalent network equation of a single slot array in free space must be taken into consideration first. According to the principle of complementary surface and duality, it is possible to make a single slot array in free space in Fig. 2(a) equivalent to the equivalent magnetic current on both sides of the PEC in Fig. 2(b). \bar{E}_{t1} and \bar{H}_{t1} denote the total field on the right side of PEC. Fig. 2(a) can also be equivalent to Fig. 2(c) according to Babinet's principle. When the magnetic dipole array is exposed to incident waves \bar{E}^i and \bar{H}^i , the total radiation field in Fig. 2(c) is:

$$\bar{E}_{tm} = \bar{E}^i + \bar{E}_{sm}, \quad \bar{H}_{tm} = \bar{H}^i + \bar{H}_{sm} \quad (1)$$

where \bar{E}_{sm} and \bar{H}_{sm} represent the scattered field produced by magnetic current $M^{(2)}(l)$ (or $V^{(2)}$) on the magnetic conductor. According to Babinet's principle, the total field on the right side of array in Fig. 2(a) can be expressed as:

$$\bar{E}_{t1} = -\bar{E}_{sm}, \quad \bar{H}_{t1} = -\bar{H}_{sm} \quad (2)$$

It can be observed from Eqs. (1) and (2) that \bar{E}_{t1} and \bar{H}_{t1} on the right side of the original slot are the negative values of the scattered field generated by magnetic current $M^{(2)}(l)$ in free space in Fig. 2(c). Corresponding to the scattered field produced when the magnetic current goes upward in Fig. 2(c), \bar{E}_{t1} and \bar{H}_{t1} are equal to the scattered field resulting from the magnetic current on the left side of PEC in Fig. 2(b).

According to the image theory, the image source of the magnetic current on the left side of PEC is the same as the original magnetic current. \bar{E}_{t1} and \bar{H}_{t1} are equal to the scattered field from $2M^{(1)}(l)$ in free space.

$$2M^{(1)}(l) = M^{(2)}(l), \quad 2V^{(1)} = V^{(2)} \quad (3)$$

where $V^{(1)}$ and $V^{(2)}$ are the magnetic current $M^{(1)}(l)$ and $M^{(2)}(l)$ of the element reference point, respectively. Suppose that the direction of magnetic current $M^{(2)}(l)$ in Fig. 2(c) is

$\bar{P}_-^{(1)}$ and that the directions of magnetic current on the left and right sides in Fig. 2(b) are respectively $\bar{P}_-^{(1)}$ and $\bar{P}_+^{(1)}$. Fig. 2(c) shows the scattering of the incident field impinging on the magnetic dipole array (magnetic conductor). The tangential field component of the sum of the incident and scattered fields in the magnetic conductor is zero as:

$$(\bar{H}^i + \bar{H}_{sm}) \cdot \bar{P}_-^{(1)} = 0 \quad (4)$$

According to Eq. (3), the scattering magnetic field generated by the magnetic current on the right-side of PEC in Fig. 2(b) is $-\bar{H}_{sm}$, and the tangential field component H_{sr} in the direction of $\bar{P}_+^{(1)}$ of the left-side magnetic current can be written as:

$$H_{sr} = -\bar{H}_{sm} \cdot \bar{P}_+^{(1)} = \bar{H}_{sm} \cdot \bar{P}_-^{(1)} \quad (5)$$

As the magnetic currents on the left and right sides of PEC are opposite in direction, the total scattered field produced by the magnetic current on the left side of PEC in Fig. 2(b) is \bar{H}_{sm} . The tangential field component H_{sl} of this field with the left-side magnetic current flowing along $\bar{P}_-^{(1)}$ is expressed as:

$$H_{sl} = \bar{H}_{sm} \cdot \bar{P}_-^{(1)} \quad (6)$$

In Fig. 2(b), the tangential component of the incident magnetic field \bar{H}^i with the left-side magnetic current flowing along $\bar{P}_-^{(1)}$ is expressed as:

$$H_{it} = 2\bar{H}^i \cdot \bar{P}_-^{(1)} \quad (7)$$

In combination with Eqs. (5) and (6), the expression is:

$$H_{it} + H_{sr} + H_{sl} = 2(\bar{H}^i + \bar{H}_{sm}) \cdot \bar{P}_-^{(1)} = 0 \quad (8)$$

Equation (8) represents the relationship between the related magnetic fields in Fig. 2(b), which is valid for any element in the array. With the reference element only taken into account, the physical concept of Eq. (8) means that the sum of the total tangential incident magnetic and scattered magnetic fields

of magnetic currents in the directions of $\bar{P}_-^{(1)}$ and the scattered

magnetic field of magnetic current in the direction of $\bar{P}_+^{(1)}$ is zero in Fig. 2(b). Eq. (8) derived from the principle of complementary surface and Babinet's theory demonstrates the physical nature of the original slot array in Fig. 2(a).

$-\bar{H}_{sm}$ in Eq. (5) represents the total scattered magnetic field produced by the magnetic current on the right side of PEC in Fig. 2(b). Supposing that this magnetic field is \bar{H}_{rt}^s ,

$$H_{sr} = \bar{H}_{rt}^s \cdot \bar{P}_+^{(1)} \quad (9)$$

\bar{H}_{sm} in Eq. (6) represents the total scattered magnetic field generated by the magnetic current on the left side of PEC. Supposing that this magnetic field is \bar{H}_{lt}^s ,

$$H_{sl} = \bar{H}_{lt}^s \cdot \bar{P}_-^{(1)} \quad (10)$$

In Eq. (7), the total incident magnetic field $2\bar{H}^i$, which is in the position of the left magnetic current, is produced by the incident magnetic field under the condition of PEC. Supposing that this magnetic field is \bar{H}_t^i ,

$$H_{it} = \bar{H}_t^i \cdot \bar{P}_-^{(1)} \quad (11)$$

The substitution of Eqs. (9)–(11) into Eq. (8) leads to:

$$\bar{H}_t^i \cdot \bar{P}_-^{(1)} = -\bar{H}_{lt}^s \cdot \bar{P}_-^{(1)} - \bar{H}_{rt}^s \cdot \bar{P}_+^{(1)} \quad (12)$$

In Eq. (12), the left and right sides respectively represent the total tangential magnetic field acting on the left and right magnetic dipole arrays and moving in the direction of the reference array, as shown in Fig. 2(b). As a result, the total tangential magnetic field is zero in the sense of physical. Suppose

that $M^{(1')t}(l) / M^{(1')t}(\bar{R}^{(1')})$ is the normalized transmitting

magnetic current from the left (or right) reference element in the infinite free space. Similar to the test function in MoM, it has no clear physical meaning. The multiplication by the current on both sides of Eq. (12) and integration on the element leads to:

$$\begin{aligned} & \frac{1}{M^{(1')t}(\bar{R}^{(1')})} \int_{ele} \bar{H}_t^i \cdot \bar{P}_-^{(1)} M^{(1')t}(l) dl \\ &= \frac{-1}{M^{(1')t}(\bar{R}^{(1')})} \int_{ele} \bar{H}_{lt}^s \cdot \bar{P}_-^{(1)} M^{(1')t}(l) dl \\ & \quad - \frac{1}{M^{(1')t}(\bar{R}^{(1')})} \int_{ele} \bar{H}_{rt}^s \cdot \bar{P}_-^{(1)} M^{(1')t}(l) dl \quad (13) \end{aligned}$$

The field components in Eq. (13) are dual to the corresponding terms of dipole array. Eq. (13) can be rewritten as:

$$I^i = -I' - I'' \quad (14)$$

where,

$$\begin{aligned} I^i &= \frac{1}{M^{(1')t}(\bar{R}^{(1')})} \int_{ele} \bar{H}_t^i \cdot \bar{P}_-^{(1)} M^{(1')t}(l) dl \\ I' &= \frac{1}{M^{(1')t}(\bar{R}^{(1')})} \int_{ele} \bar{H}_{lt}^s \cdot \bar{P}_-^{(1)} M^{(1')t}(l) dl \\ I'' &= \frac{-1}{M^{(1')t}(\bar{R}^{(1')})} \int_{ele} \bar{H}_{rt}^s \cdot \bar{P}_-^{(1)} M^{(1')t}(l) dl \end{aligned} \quad (15)$$

The direction of I^i and I' conforms with $\bar{P}_-^{(1)}$ and that of I'' with $\bar{P}_+^{(1)}$. Suppose:

$$Y_1^{1,1} = \frac{-I'}{V^{(1)}}, \quad Y_2^{1,1} = \frac{-I''}{V^{(1)}} \quad (16)$$

The substitution of Eq. (16) into Eq. (14) leads to:

$$I^i = (Y_1^{1,1} + Y_2^{1,1}) V^{(1)} = Y^{1,1} V^{(1)} \quad (17)$$

Equation (17) represents the network of a single slot array in free space. Therefore, Fig. 2(b) can be equivalent to a magnetic dipole array interconnected with both sides of PEC.

The maximum electric field of FSS determines its power capacity. When the maximum electric field exceeds breakdown field strength of the surrounding air or dielectric, the FSS will be broken down, affecting its spatial filtering characteristics. The magnetic current distribution function calculated in Section 3 can be further used to calculate the maximum electric field in this section.

The slot array usually analyzes the incident magnetic field \bar{H}^i , and the induced current is:

$$I^i = 2 [\perp H^i \cdot \perp P_0^t + \parallel H^i \cdot \parallel P_0^t] \quad (18)$$

where $\parallel \hat{n}$ is the wave vector reference direction; $\perp P_0^t$ and $\parallel P_0^t$ respectively represent the vertical and horizontal transmitting functions:

$$\parallel P_0^t = \parallel \hat{n}_0 \cdot \bar{P}^{(0)} \int_{element} I^t(l) e^{j\beta_0 l \bar{P}^{(0)} \bar{r}_0} dl \quad (19)$$

The maximum field strength of slot type element FSS is:

$$E_{B \max} = \alpha \frac{V_{B \max}}{w} = \alpha \frac{I^i}{w \cdot G_A} \quad (20)$$

where G_A represents the real part of the scanning admittance of the FSS element under resonance conditions [13], and α is the shape factor.

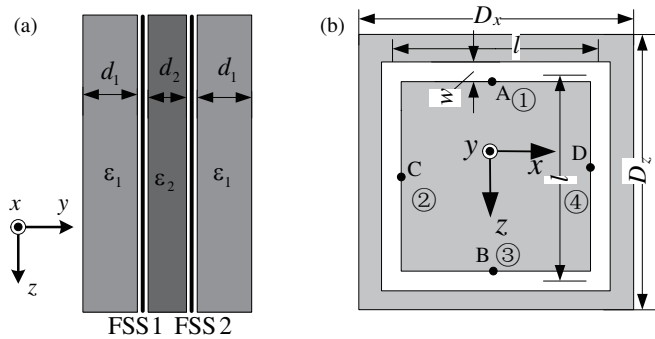


FIGURE 3. Topology of the square slot ring FSS, $\epsilon_1 = 1.3$, $\epsilon_2 = 1.9$. $w = 2.25 \times 10^{-4}$, $l = 6.675 \times 10^{-3}$, $l_1 = l/2$, $d_1 = 9 \times 10^{-3}$, $d_2 = 5.5 \times 10^{-3}$ $D_x = D_z = 7.2 \times 10^{-3}$ (unit: m). (a) side view, (b) top view.

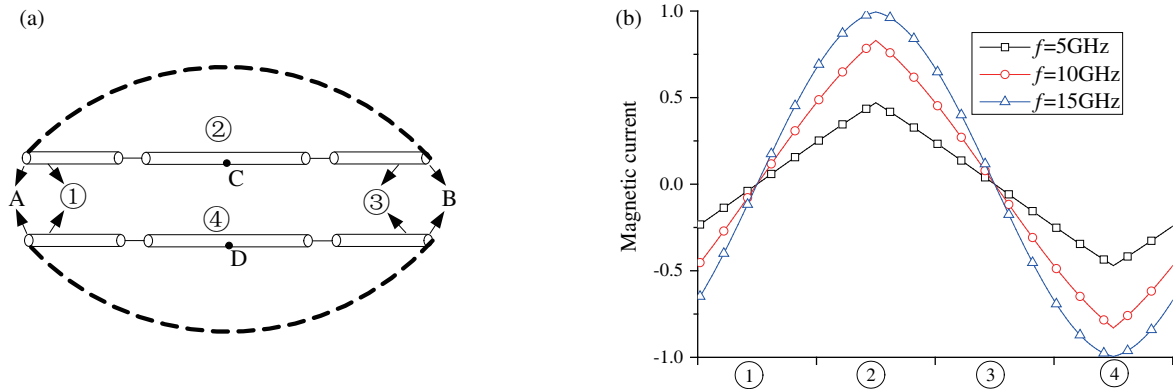


FIGURE 4. (a) Approximate magnetic current distribution model of Fig. 3(b), (b) Approximate magnetic current.

3. NUMERICAL EXAMPLES

As discussed in the introduction, this method is based on Munk’s scheme. However, the two main different points are: a) The current (or magnetic current) distribution of loop-type FSS element is approximated as whole domain sinusoidal function. b) The receiving current is used as basis function and test function to eliminate the calculation of transmitting current. The construction of the efficient equivalent transmission line method for FSS can be done by following the procedure described in [14].

3.1. Transmission Coefficient of Square Slot Ring FSS

The first example is a square slot loop FSS as depicted in Fig. 1. For the patch array, the current along the strip is calculated, and the Munk’s scheme in this case is based on the mutual impedance matrix. However, for the slot array, the magnetic current along the slot is analyzed, and the Munk’s scheme in this case is based on the mutual admittance matrix. Suppose that the magnetic field is along z -axis. As the geometric and excitation is symmetric about center line A-B, the magnetic current at points A and B should be zero. Consequently, the magnetic current distribution can be approximated as sinusoidal function with extreme points at Points C and D as shown in Fig. 4.

Section ①,

$$I_1(z) = \sin[\beta(z - 0.5l)] \quad z \in (0, l) \quad (21)$$

Section ②,

$$I_2(z) = \begin{cases} \sin[\beta(z + 0.5l)] & z \in (0, 0.5l) \\ \sin[\beta(1.5l - z)] & z \in (0.5l, l) \end{cases} \quad (22)$$

Section ③,

$$I_3(z) = \sin[\beta(-z + 0.5l)] \quad z \in (0, l) \quad (23)$$

Section ④,

$$I_4(z) = \begin{cases} -\sin[\beta(z + 0.5l)] & z \in (0, 0.5l) \\ -\sin[\beta(1.5l - z)] & z \in (0.5l, l) \end{cases} \quad (24)$$

where propagation constant is $\beta = \omega\sqrt{\mu_0\epsilon_0\epsilon_r}$, and the effective dielectric constant is $\epsilon_r = (\epsilon_1 + \epsilon_2)/2$. The magnetic current distribution is plotted in Fig. 4(b). The transmission coefficient is shown in Fig. 5(b), together with the comparison of HFSS and measurement. The CPU time is about 0.3 s and 515 s for the proposed method and HFSS, respectively. It can be observed that the normalized magnetic current on the closed square slot loop remains almost the same from 5 GHz to 15 GHz.

The good agreement between the proposed method and HFSS is inspiring. It provides a simple approximation of the magnetic current distribution on square slot. In fact, since the currents at Points A and B are equal to zero, we can “truncate” the square slot at points A and B, and “straighten”

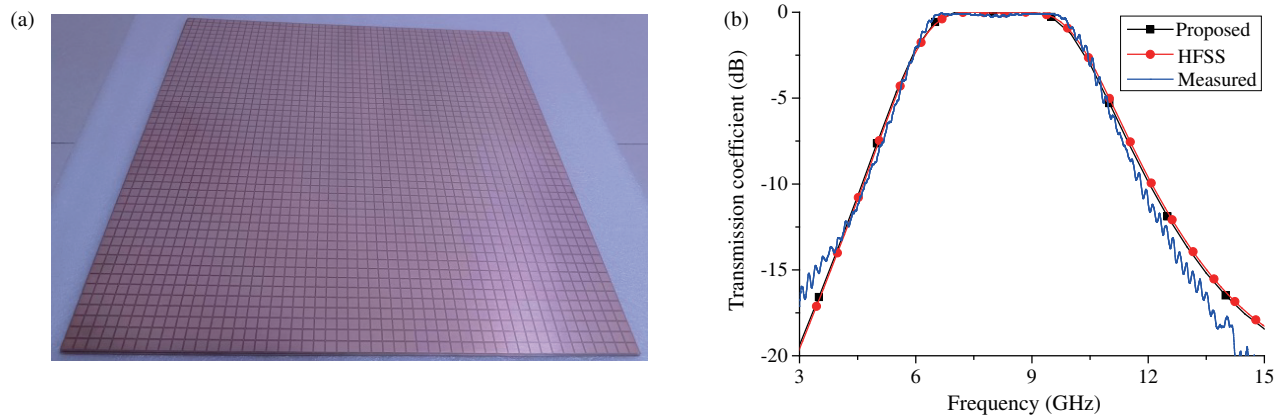


FIGURE 5. (a) Fabricated prototype of Fig. 3. (b) Transmission coefficient.

the two parts of A-C-B and A-D-B, respectively. The magnetic current distribution on these two parts is similar to the current distribution on dipole antenna. Consequently, a sinusoidal function is usually used as the corresponding approximate current distribution.

3.2. Transmission Coefficient of Triangle Slot Ring FSS

Inspired by the analysis and calculation of square slot ring FSS, the triangle slot ring FSS is studied in this section (Fig. 6). Suppose that the magnetic field is along z -axis. Because the z -coordinates of Points C and D are equal, the cumulative contribution of the magnetic field to the magnetic current of the two points should be the same with the extreme points. Similar to the analysis of the square slot ring FSS, the magnetic current should be zero at $2/3$ of Section 1 (Point A) and $1/3$ of Section 3 (Point B). Consequently, we can “truncate” the triangle slot at points A and B, and “straighten” the two parts of A-C-B and A-D-B as shown in Fig. 8. These two parts can also be equivalent to dipole antenna. The corresponding magnetic current distribution can be written as:

Section ①,

$$I(z) = \sin[\beta(z - 0.75l)] \quad z \in (0, l) \quad (25)$$

Section ②,

$$I(z) = \begin{cases} \sin[\beta(z + 0.25l)] & z \in (0, 0.5l) \\ \sin[\beta(0.75l - z)] & z \in (0.5l, l) \end{cases} \quad (26)$$

Section ③,

$$I(z) = \sin[\beta(-z + 0.25l)] \quad z \in (0, l) \quad (27)$$

The magnetic current distributions are shown in Fig. 7. The transmission coefficient are depicted in Fig. 8. The proposed method can accurately predict the transmission characteristic of the triangle slot ring FSS in the low frequency band and pass-band. The deviation in the high frequency band mainly results from the low accuracy of magnetic current distribution. However, the CPU time of the proposed method is about 0.06% of HFSS.

The examples of square slot ring FSS and triangle slot ring FSS confirm that, in the low frequency band, the magnetic cur-

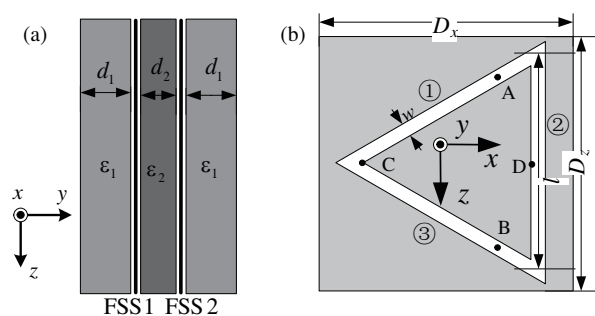


FIGURE 6. Topology of the triangle slot ring FSS, $\epsilon_1 = 1.3$, $\epsilon_2 = 1.9$. $w = 2.25 \times 10^{-4}$, $l = 7 \times 10^{-3}$, $d_1 = 9 \times 10^{-3}$, $d_2 = 5.5 \times 10^{-3}$, $D_x = D_z = 7.2 \times 10^{-3}$ (unit: m). (a) Side view, (b) top view.

rent distribution along the closed loop has two extreme points at the two endpoints in the symmetry of the element magnetic field, and two zero points at the center position of the circumference of the element along the direction of the magnetic field. We can “truncate” the loop at the zero points and “straighten” the two parts. The magnetic current distribution on these two parts is similar to the current distribution on dipole antenna. A sinusoidal function can be used as the corresponding approximation. When the shape function in Munk’s scheme is calculated, the normalized magnetic current is applied other than the actual magnetic current. In other words, with high precision normalized magnetic current distribution of FSS element, high precision transmission coefficient can be calculated.

According to the above magnetic current approximation method, one can approximate the magnetic current distribution of other type FSS elements which will be discussed in our future work. The deviation of the transmission coefficients in the high frequency band can be optimized by choosing other expression for the magnetic current. With the increase of the frequency, the electric size of the FSS element is increased. It should have more zero points and extreme points along the loop. The simple sinusoidal function is unable to approximate the high frequency component of the magnetic current. A simple and general basis function is deserved to be studied. The proposed method can also be applied to the analytical multimodal equivalent network method.

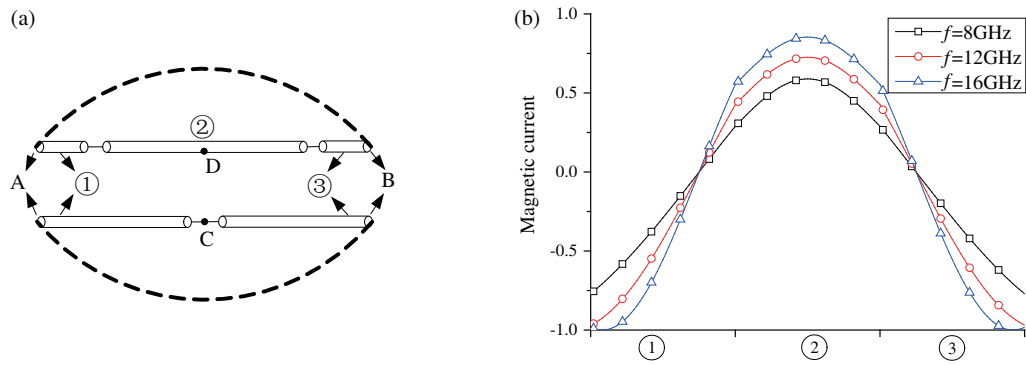


FIGURE 7. (a) Approximate magnetic current distribution model of Fig. 6(b). (b) Approximate magnetic current.

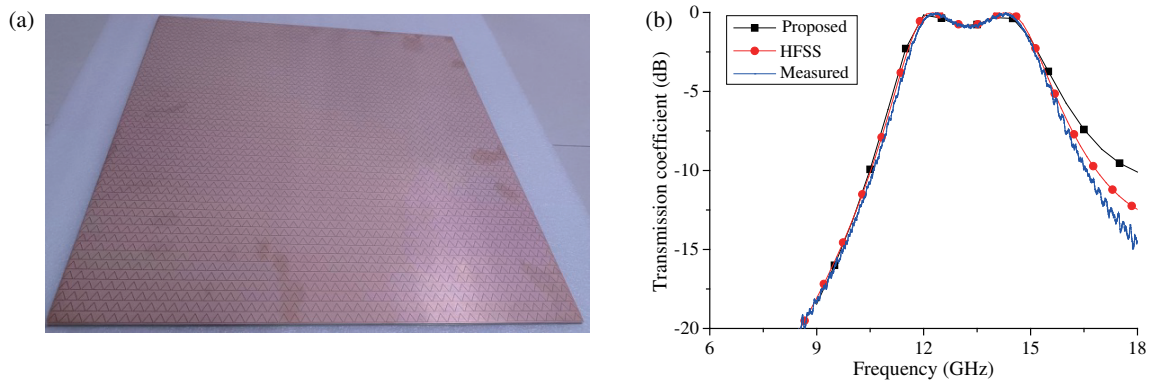


FIGURE 8. (a) Fabricated prototype of Fig. 6. (b) Transmission coefficient.

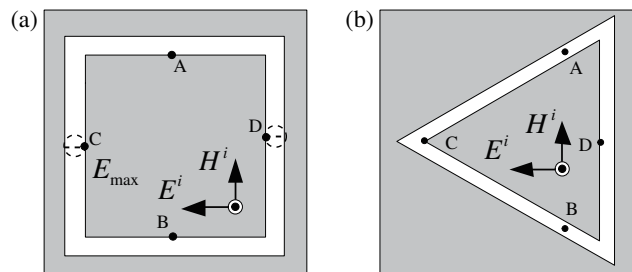


FIGURE 9. Electric field breakdown diagram. (a) Rectangle slot ring FSS. (b) Triangle slot ring FSS.

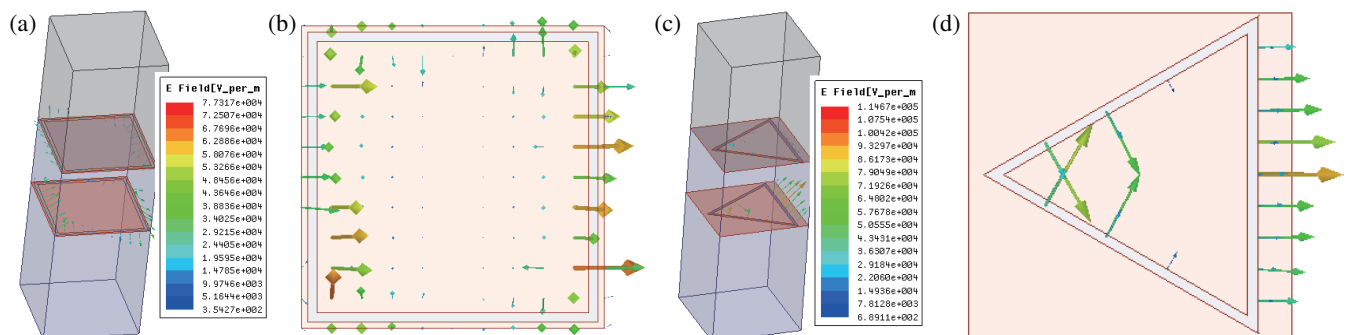


FIGURE 10. Simulated slot electric field distribution. (a) General view and top view of rectangle slot ring FSS, (b) general view and top view of triangle slot ring FSS.

3.3. Power Handling

To facilitate the comparison with HFSS electromagnetic simulation results, the average power of incident electromagnetic wave in Figs. 3 and 6 is set as 1 W.

For rectangular slot ring FSS, as shown in Fig. 5, the corresponding positions of the maximum magnetic current are point C and point D. These two points are the positions of the maximum voltage, as shown in Fig. 9(a). Bring the current distribution modeled by Eqs. (18)–(22) into Eq. (26) to calculate the shape function, and then calculate the element scanning admittance to finally calculate the maximum electric field of the element as 81.2 kV/m. Similarly, for the triangle slot ring FSS show in Fig. 6, the maximum magnetic current is located at point D. According to the above solution process, the corresponding maximum electric field value is 116 kV/m.

In order to verify the correctness of this method, HFSS is used to simulate the slot electric field in Figs. 3 and 6. As shown in Fig. 10, the maximum electric fields are 77.3 kV/m and 114.67 kV/m, respectively. The value and position of the maximum electric field are approximately consistent with the proposed method, which verifies the efficiency of the proposed method.

4. CONCLUSION

An approximate analytical method is proposed to study the power handling of slot type frequency selective surface. The physical nature of the corresponding periodic scattered matrix is deduced. By multiplying the normalized transmitting magnetic current on both sides of the equation of magnetic field where the total tangential component is zero and integrated on the element, the field equations are transformed into circuit equations for the convenience of calculation. A simple sinusoidal function is used to approximate the magnetic current distribution for slot loop FSS element. Two typical examples of dual layer hybrid radomes show that the transmission coefficient and the maximum electric field calculated by the proposed method are in good agreement with HFSS. The CPU time of this method and HFSS is about 0.3 s and 515 s respectively.

ACKNOWLEDGEMENT

The work was supported by the National Science Found for Distinguished Young under Grants No. 52025072 and National Key R&D Program of China (2021YFF1500100).

REFERENCES

- [1] Molero, C., R. Rodriguez-Berral, F. Mesa, F. Medina, M. Memarian, and T. Itoh, "Planar resonant blazed gratings from a circuit model standpoint," *IEEE Transactions on Antennas and Propagation*, Vol. 68, No. 4, 2765–2778, Apr. 2020.
- [2] Luo, K., Y. Yi, Z. Cai, F. Lu, X. Zhou, and B. Chen, "An efficient spectral WLP-FDTD algorithm for periodic structures," *IEEE Transactions on Antennas and Propagation*, Vol. 64, No. 10, 4468–4471, Oct. 2016.
- [3] Langley, R. J. and E. A. Parker, "Equivalent-circuit model for arrays of square loops," *Electronics Letters*, Vol. 18, No. 7, 294–296, 1982.
- [4] Marcuvitz, N., *Waveguide Handbook*, McGraw, New York, USA, 1951.
- [5] Langley, R. J. and E. A. Parker, "Double-square frequency-selective surfaces and their equivalent-circuit," *Electronics Letters*, Vol. 19, No. 17, 675–677, 1983.
- [6] Li, M., S. Xiao, Y.-Y. Bai, and B.-Z. Wang, "An ultrathin and broadband radar absorber using resistive FSS," *IEEE Antennas and Wireless Propagation Letters*, Vol. 11, 748–751, 2012.
- [7] Costa, F., A. Monorchio, and G. Manara, "Analysis and design of ultra thin electromagnetic absorbers comprising resistively loaded high impedance surfaces," *IEEE Transactions on Antennas and Propagation*, Vol. 58, No. 5, 1551–1558, May 2010.
- [8] Ferreira, D., R. F. S. Caldeirinha, I. Cuinas, and T. R. Fernandes, "Square loop and slot frequency selective surfaces study for equivalent circuit model optimization," *IEEE Transactions on Antennas and Propagation*, Vol. 63, No. 9, 3947–3955, Sep. 2015.
- [9] Costa, F., A. Monorchio, and G. Manara, "Efficient analysis of frequency-selective surfaces by a simple equivalent-circuit model," *IEEE Antennas and Propagation Magazine*, Vol. 54, No. 4, 35–48, Aug. 2012.
- [10] Molero, C., R. Rodriguez-Berral, F. Mesa, and F. Medina, "Dynamical equivalent circuit for 1-D periodic compound gratings," *IEEE Transactions on Microwave Theory and Techniques*, Vol. 64, No. 4, 1195–1208, Apr. 2016.
- [11] Mesa, F., M. Garcia-Vigueras, F. Medina, R. Rodriguez-Berral, and J. R. Mosig, "Circuit-model analysis of frequency selective surfaces with scatterers of arbitrary geometry," *IEEE Antennas and Wireless Propagation Letters*, Vol. 14, 135–138, 2015.
- [12] Munk, B. A., *Frequency Selective Surfaces: Theory and Design*, 79–124, Wiley, New York, USA, 2000.
- [13] Luo, K., Y. Yi, Z.-Y. Zong, B. Chen, X. Zhou, and Y. Duan, "Approximate analysis method for frequency-selective surface based on kirchhoff-type circuit," *IEEE Transactions on Antennas and Propagation*, Vol. 66, No. 11, 6076–6085, Nov. 2018.
- [14] Luo, K., J. Meng, D. Zhu, S. Ge, and J. Han, "Approximate analytical method for hexagonal slot frequency selective surface analysis," *International Journal of Rf and Microwave Computer-aided Engineering*, Vol. 31, No. 9, Sep. 2021.
- [15] Li, L., Y.-W. Liu, K. K. Mei, and K.-W. Leung, "Applications of the maxwellian circuits to linear wire antennas and scatterers," *IEEE Transactions on Antennas and Propagation*, Vol. 54, No. 10, 2725–2730, Oct. 2006.
- [16] Mei, K. K., "Theory of Maxwellian circuits," *The Radio Science Bulletin*, No. 303, 6–13, Sep. 2003.
- [17] Shen, W., C. Xue, K. K. Mei, and J. Lin, "Maxwellian circuits of conducting circular loops," *IEEE Transactions on Antennas and Propagation*, Vol. 59, No. 10, 3848–3854, Oct. 2011.
- [18] Schelkunoff, S. A. and H. T. Friis, *Antennas: Theory and Practice*, Wiley, New York, USA, 1952.
- [19] Zhang, J., M. Lin, Z. Wu, L. Ding, L. Bian, and P. Liu, "Energy selective surface with power-dependent transmission coefficient for high-power microwave protection in waveguide," *IEEE Transactions on Antennas and Propagation*, Vol. 67, No. 4, 2494–2502, Apr. 2019.
- [20] Xie, H., T. Hu, Z. Wang, Y. Yang, X. Hu, W. Qi, and H. Liu, "A physics-based HIE-FDTD method for electromagnetic modeling of multi-band frequency selective surface," *Progress In Electromagnetics Research*, Vol. 173, 129–140, 2022.
- [21] Zhao, C., C.-F. Wang, and S. Aditya, "Power-dependent frequency-selective surface: concept, design, and experiment," *IEEE Transactions on Antennas and Propagation*, Vol. 67, No. 5, 3215–3220, May 2019.

[22] Li, X., Z. Zhou, Q. Wang, and J. Zhang, "A polarization conversion radome for high-power microwave applications," *IEEE An-*

tennas and Wireless Propagation Letters, Vol. 18, No. 6, 1096–1099, Jun. 2019.